THE ASTROPHYSICAL JOURNAL, 276:79–91, 1984 January 1

OPTICAL LINE EMISSION ASSOCIATED WITH THE RADIO GALAXY 4C 26.42 IN THE CLUSTER OF GALAXIES ABELL 1795

WIL VAN BREUGEL,[1,2] TIMOTHY HECKMAN,[2,3,4] AND GEORGE MILEY[4,5]
Received 1983 March 11; accepted 1983 June 16

ABSTRACT

Extended optical emission-line gas has been detected from the radio galaxy 4C 26.42. This gas is morphologically related to the radio continuum distribution. A detailed study of the radio and optical emission is presented comprising VLA maps at 20, 6, and 2 cm, broad- and narrow-band optical images, and long-slit spectra. These data demonstrate a clear connection between the thermal (optically emitting) and relativistic (radio-emitting) media in this galaxy. The extranuclear line emission occurs predominantly along the radio source boundary, brightens near an indentation and brightness enhancement in the radio source, and is anti-correlated with the radio polarization. Physical parameters deduced for the two media also suggest a close physical relationship. The enhanced line emission along the boundaries and the anticorrelation between the presence of line emission and the radio polarization suggest that the source is depolarized by an inhomogeneous magnetoionic screen surrounding the source. Assuming a simple model, we derive a rough estimate for the typical scale size of the irregularities in this material. X-ray data indicate that 4C 26.42, which is identified with the dominant cD galaxy in the rich cluster Abell 1795, is immersed in a relatively cool and dense (thermally unstable) gaseous halo. The radio source is expected to entrain and compress this gas, and subsequent rapid cooling would then naturally produce bright optical line emission around the radio source boundary. Slow, subsonic motion of the cD galaxy with respect to the surrounding intracluster medium would account for the kinematics of the line-emitting gas (velocities decline by 400–500 km s^{-1} outside the nucleus) and the asymmetric brightness we observe in the radio lobes and the associated line emission.

Subject headings: galaxies: clustering — radio sources: galaxies

I. INTRODUCTION

Much progress in the study of extragalactic radio sources has been made in the past few years, because of the increase in resolution and sensitivity of radio interferometers. To infer the physical conditions in radio sources from radio data alone, however, involves many assumptions, and it is important to search for other possible observational constraints on models of radio sources.

We therefore embarked on a search for optical line emission associated with extended extragalactic radio sources using modern imaging and spectroscopic techniques. From extended optical line emission, important parameters such as the temperature, density, pressure, filling factors, ionization mechanisms, and kinematics of the line-emitting gas may be derived. The radio/optical interrelations may then provide a better insight into the physical conditions within radio sources and in their environment, independent of the usual assumptions that have to be made when analyzing radio data alone. We have recently studied extended optical line emission from the radio galaxies 3C 277.3 (Coma A) (Miley *et al.* 1981), 3C 305 (Heckman *et al.* 1982), and 3C 293 (van Breugel *et al.* 1984*a*) and have shown that in these cases the line-emitting gas and radio sources are clearly related. In the present paper we report the discovery of extended optical line emission associated with the radio source 4C 26.42 (1346+268). This source has been identified with the dominant central galaxy in the cluster Abell 1795 (Merkelijn 1972; Owen, Rudnick, and Peterson 1977). It is a luminous X-ray source (McKee *et al.* 1980) and was originally included in the survey of emission-line gas in cD galaxies carried out by Heckman (1981). Some global properties of 4C 26.42 are summarized in Table 1.

The line emission was first detected in narrow-band images in the light of Hα + [N II]. Comparisons with the existing radio map of 4C 26.42 (Bridle and Fomalont 1978) showed that the optical and radio emission were related and stimulated us to make further observations. First, using the Very Large Array (VLA) we have obtained multifrequency higher quality radio maps which have resolutions comparable to that of our emission-line images. Second, we applied slit spectroscopy to study the kinematics and physical state of the line-emitting gas.

In § II we describe the various observations. In § III the results are presented, which are then discussed in § IV.

II. OBSERVATIONS AND REDUCTION

Various parameters pertaining to the radio and optical observations are summarized in Tables 2 and 3, respectively.

a) Radio

4C 26.42 was observed at 1465 MHz (20 cm), 4885 MHz (6 cm), and 14,965 MHz (2 cm) using the VLA (Thompson *et al.* 1980) in the A, B, and C configurations, respectively. At

[1] Steward Observatory, University of Arizona, Tucson (work partially completed while at Kitt Peak National Observatory).
[2] Visiting Astronomer at the National Radio Astronomy Observatory, which is operated by Associated Universities, Inc., under contract to the National Science Foundation.
[3] Astronomy Program, University of Maryland, College Park.
[4] Visiting Astronomer at Kitt Peak National Observatory, which is operated by AURA, Inc., under contract to the National Science Foundation.
[5] Leiden Observatory, Leiden University, The Netherlands.

TABLE 1

GLOBAL PROPERTIES OF 4C 26.42 (1346+268)

Parameter	Value	Ref.
Radio		
Flux density (1415 MHz)	0.98 Jy	1
Monochromatic power (1415 MHz)	6.9×10^{24} W Hz^{-1}	1
Total radio luminosity	8.7×10^{34} W	2
Spectral index $(S_\nu)^{-\alpha}$	1.0	1
Size (max., min.)	$2'' \times 12''$	2
Position angle major axis	$\sim 18°$	2
Optical		
Redshift	0.0630	3
Distance	256 Mpc[a]	
Linear/angular size ratio	1.1 kpc arcsec^{-1} [a]	
Galaxy type	cD	4
M_v	−23.2	4
Galaxy size (max., min.)	$70'' \times 38''$	2
Position angle major axis	$14° \pm 5°$	2

[a] $H_0 = 75$ km s^{-1} Mpc^{-1}, $q = 0.5$.

REFERENCES:—(1) Colla *et al.* 1975. (2) This paper. (3) Sargent 1973; Colla *et al.* 1975. (4) Olsen 1970.

each of these wavelengths the sampling of the source structure is comparable so that high-resolution (1.″3) maps could be made to intercompare the total and polarized intensity distributions. The source was also observed at 6 cm in the A configuration, yielding even higher resolution (0.″3).

For all observations 3C 286 was used as the primary calibrator for the flux density and the absolute polarization position angle. The secondary calibrator, 3C 287, was observed for ~2 minutes every 15–20 minutes to monitor amplitude and phase fluctuations and to calibrate the polarization.

Reduction of the data was standard, using the NRAO Astronomical Image Processing System programs at the VLA and the Charlottesville VLA reduction system and image display facilities of the Westerbork reduction system, both at Leiden University. The maps were CLEANed and restored using circular Gaussian beams which best fitted the instrumental beams: 1.″3 (full width half-maximum, FWHM) for the 20 cm, 6 cm, 2 cm observations in the A, B, and C configurations and 0.″3 (FWHM) in the A configuration 6 cm observations. The A configuration maps were also "self-calibrated" to improve dynamic range.

TABLE 2A

LOG OF THE RADIO OBSERVATIONS
POINTING POSITION (1950): R.A. = $13^h46^m33^s.971$; DECL. = 26°50′28.″0.4

Configuration[a]	Date	Frequency (MHz)	Bandwidth (MHz)	Resolution (arcsec)
A	1982 Feb	4885	50	0.3
A	1982 Feb	1465	50	1.3
B	1981 Jul	4885	50	1.3
C	1981 Oct	14965	50	1.3

TABLE 2B

CALIBRATORS

Frequency (MHz)	3C 286[b] Flux Density (Jy)	3C 287[c] Flux Density (Jy)
1465	14.51	6.84
4885	7.41	3.28
14965	3.44	1.40

[a] See Thompson *et al.* 1980.
[b] Primary calibrator for flux density and polarization position angle.
[c] Secondary calibrator.

b) Optical

i) *Imaging*

Optical images of 4C 26.42 were obtained using the intensified silicon intensified target (ISIT) vidicon video camera (Robinson *et al.* 1979) on the 2.1 m telescope at Kitt Peak National Observatory (see Table 3).

The emission-line gas associated with 4C 26.42 was mapped using narrow-band (55 Å) filters. The observations and reduction procedures have been described by Heckman (1981).

Also a broad-band (~900 Å) exposure was taken through a red filter for general morphological information.

ii) *Spectroscopy*

To obtain information on the properties and kinematics of the emission-line gas, long-slit spectra were taken with the High-Gain Video Spectrometer (HGVS) and Cryogenic Camera in conjunction with the Ritchey–Chrétien spectrograph on the KPNO 4 m telescope. The CCD-based Cryogenic Camera is more sensitive than the HGVS except for wavelengths below ~4500 Å, whereas the HGVS has the advantage of better wavelength resolution. Details concerning the specifications and the gratings used are given in Table 3. The observations and reductions were conducted in a standard way (see, for example, Heckman *et al.* 1981, 1982; Balick and Heckman 1983).

4C 26.42 was observed with the HGVS in 1981 June, using a grating covering the [O II] λλ3726, 3729 doublet and with a resolution of 2.2 Å (~165 km s^{-1}). Two parallel slit positions ~2″ apart in position angle 145° were used to cover most of the line emission seen in our Hα + [N II] image in Figure 6. The [O II] λ3727 line is a doublet (λ3726.1 and λ3728.8), which is blended in our spectra of 4C 26.42. We have derived the intrinsic line widths using a Gaussian deconvolution technique and assuming an intensity ratio of the doublet of ~1 (equivalent to a density of ~600 cm^{-3} of the emission-line gas). The derived widths are relatively insensitive to these assumptions, and we estimate that the uncertainties are $\lesssim 15\%$. The uncertainty in the relative velocities due to the blend is ±35 km s^{-1} at most.

In 1981 November we observed 4C 26.42 using the Cryogenic Camera with the slit in position angle 162° and centered at the nucleus. We have used the spectrophotometric data on the nucleus of 4C 26.42 obtained by Wilkinson, Hine, and Sargent (1981) to roughly calibrate our data in terms of relative flux. However, accurate relative or absolute spectrophotometry is not possible with the Cryogenic Camera, and errors of 20% or 30% between the red and blue ends of the spectrum are likely.

The density-sensitive ratio of [S II] λ6716 to λ6731 has been measured by deblending the doublet assuming Gaussian line profiles of equal width for the two components. Since each of

TABLE 3A

LOG OF THE OPTICAL OBSERVATIONS

	Imaging		Slit Spectroscopy	
Type of Observation	Broad Band	Narrow Band	Low Resolution	High Resolution
Telescope	2.1 m	2.1 m	4 m	4 m
Auxiliary instrument	ISIT video camera	ISIT video camera	Cryogenic Camera	HGVS
Wavelength	6450 Å (red)	$(1+z)$ 6562 Å (Hα)	see below	see below
Bandwidth	1400 Å	55 Å	3400 Å	340 Å
Spatial resolution	1″.7	1″	2″.5	2″
Field size	130″ × 130″	130″ × 130″	3″.2 × 240″	2″ × 166″
Pixel size	0″.57 × 0″.57	0″.57 × 0″.57	0″.8 × 4.3 Å	1″.3 × 0.7 Å
Number of pixels	256 × 256	256 × 256	300 × 800	128 × 512
Date	1981 Mar	1981 Jan	1981 Nov	1981 Jun
Purpose of observations	morphology of galaxy	morphology of emission-line gas	kinematics, ionization state, and density of emission-line gas	kinematics of emission-line gas

TABLE 3B

PARAMETERS OF SLIT SPECTRA

Position Angle (Degrees)	Wavelength Coverage (Å)	Wavelength Resolution (Å)	Integration Time (minutes)	Instrument
145[a]	3604–4320	2.2	14	HGVS
145[a]	3604–4320	2.2	14	HGVS
162	4500–7900	15	20	Cryogenic Camera

[a] Two parallel slit positions offset by −1″.8. Northeast and southwest from the nucleus.

the two components was ∼25 Å wide (including instrumental broadening), the ratio could not be accurately measured, and only an upper limit could be set.

III. RESULTS

a) Radio

i) Morphology

The 20 cm, 6 cm, and 2 cm total and polarized intensity maps with 1″.3 resolution and the 6 cm maps with 0″.3 resolution are shown in Figures 1 and 2, respectively.

4C 26.42 is a relatively small (∼2 × 13 kpc) and bright ($\gtrsim$10 mJy arcsec^{-2} at 6 cm) **Z**-shaped radio source. Various radio components are labeled in Figure 2. The only compact ($\lesssim$0″.3) features are the nucleus (N) and the two components straddling it (B_1, B_2). Beyond B_1 and B_2 the source flares out and bends by almost 90°. Subsequently, the lobes do not widen significantly with distance from the nucleus. The northern lobe has a slight indentation and a higher surface brightness than in the southern lobe at a comparable distance from the nucleus, close to a region with bright optical line emission (Fig. 6).

ii) Polarization

At 20 cm no polarization was detected at a level $\gtrsim$0.15 mJy per beam (3 σ, polarized flux density). At 6 cm (1″.3 resolution) a few polarized regions were found with the percentage polarization in the lobes being only ∼3% with an uncertainty of ±1%. The percentage polarization near the nucleus (1%–2%) is very uncertain and probably mostly of instrumental origin because of the large intensity gradients here (see van Breugel and Jägers 1982). At higher resolution (0″.3, Fig. 2) the polarized regions break up into smaller patches with a much higher percentage polarization: 10%–30%, depending on the region, with an uncertainty of typically ±5%. These polarized patches are found near steep intensity gradients. Evidently the lower percentage polarization at the lower (1″.3) resolution is due to the summation within a beam size of several smaller regions ($\lesssim$0″.3) with different polarization position angles. At 2 cm the signal-to-noise ratio is relatively poor. However, the observations suggest a rather high percentage polarization near locations where some polarized emission was also detected at 6 cm.

From this scarce information it appears that while most of the source is unpolarized at *all* wavelengths (at 1″.3 resolution), in a few regions in the lobes the percentage polarization increases rapidly with wavelength: typically from $\lesssim$0.7% at 20 cm to ∼3% at 6 cm and ∼45% at 2 cm.

iii) Spectral Index

Slices along the ridge line of the 6 cm total intensity and the corresponding values for the spectral index between 6 cm and 20 cm (α_6^{20}) and between 2 cm and 6 cm (α_2^6) are shown in Figure 3. We conclude that the spectral index is relatively large over the entire source and increases with distance from the nucleus. There is no evidence for a strong self-absorbed nuclear component. Comparison of our 1″.3 VLA maps of 4C 26.42 with a 1″.5 resolution map made at 408 MHz (73 cm; Muxlow and Ilyasov 1981) furthermore shows that there is no significant curvature of the spectrum between 20 cm and 73 cm at any location at this resolution. Comparing α_6^{20} and α_2^6 in Figure 3 suggests that the spectrum in the lobes steepens significantly between 20 cm and 2 cm.

iv) Physical Parameters

We have used the 6 cm maps and the spectral index distribution to derive the various physical parameters listed in Table 4. The sizes and flux densities for the small components B_1, N, B_2, and C_2 were derived from the 0″.3 resolution 6 cm map, and the average values for the lobes and the total source, from the lower resolution (1″.3) map. The most important,

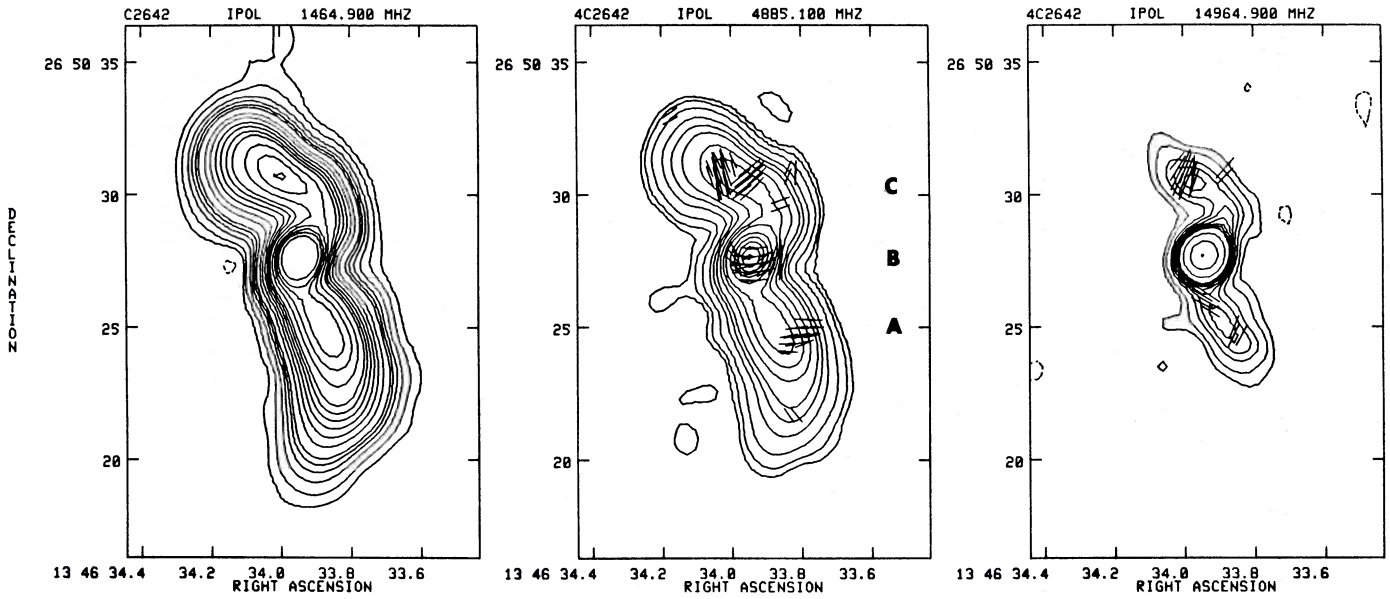

FIG. 1.—(*left*) Contour map of 4C 26.42 at 20 cm with 1.″3 × 1.″3 resolution. Contour values are: 0.15 × (−4 [*dashed*], 4, 10, 20, 30, 40, 50, 75, 100, 125, 150, 175, 200, 250, 300, 400, 500) in mJy per beam. (*middle*) Contour map of 4C 26.42 at 6 cm with 1.″3 × 1.″3 resolution. Polarization vectors are shown superposed. Contour values are: 0.15 × (−3 [*dashed*], 3, 5, 10, 20, 30, 40, 60, 80, 100, 150, 200, 250, 300, 350) in mJy per beam. The lengths of the bars are proportional to the polarized intensity: 1″ in length corresponds to 0.33 mJy per beam. (*right*) Same as Fig. 1, *middle*, at 2 cm. Contour values are: 0.3 × (−3 [*dashed*], 3, 5, 8, 10, 12, 14, 16, 18, 20, 30, 50, 75) in mJy per beam. The lengths of the bars are proportional to the polarized intensity: 1″ in length corresponds to 1.81 mJy per beam.

ad hoc, assumptions we have used (see, for example, Pacholczyk 1970) are:

1. The total energy is minimal as a function of magnetic field strength.
2. The relativistic electron and proton energies are equal.
3. The filling factor of the synchrotron emission is one.
4. The nonthermal spectrum is straight and extends from 10 MHz to 100 GHz.

b) Optical

i) *Morphology: Comparison with the Radio Maps*

The broad-band red image of the galaxy identified with 4C 26.42 is shown in Figure 4. The galaxy extends over at least 40″ × 60″ and entirely encompasses the radio source (2″ × 12″). The inner radio axis (P.A. ≈ 120°) is close to the minor axis of the galaxy (P.A. ≈ 105°), while the outer lobes (P.A. ≈ 20°) are approximately aligned with the major axis (P.A. ≈ 14°).

A contour representation of the Hα + [N II] image of 4C 26.42 is shown in Figure 5. Various features have been labeled, and their corresponding sizes and Hα + [N II] fluxes are listed in Table 5. Our value for the integrated Hα + [N II] flux is in good agreement with the spectrophotometric data reported by Wilkinson, Hine, and Sargent 1981). No [O III] λ5007 was detected, and we can set an upper limit of $F_{[O\,III]} \lesssim 8 \times 10^{-15}$ ergs cm^{-2} s^{-1} (Heckman 1981). This low [O III]/Hα intensity ratio agrees with our spectroscopic results (see below).

An overlay of the emission-line (Hα + [N II]) and radio (6 cm, 0.″3) maps is shown in Figure 6. To align the maps we have assumed exact coincidence of the radio and optical nuclei. We note the following.

1. The brightest extranuclear line emission is found predominantly along the boundaries of the radio source.
2. A bright emission-line region (K) with adjacent enhanced radio emission (C_2) is located near an indentation in the northwestern radio source boundary.

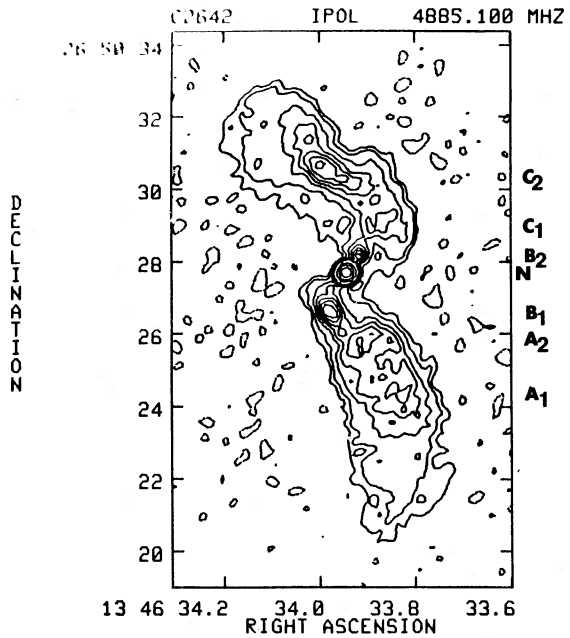

FIG. 2*a*.—Contour map of 4C 26.42 at 6 cm with 0.″3 × 0.″3 resolution. Contour values are: 0.15 × (−1 [*dashed*], 1, 2, 4, 6, 8, 10, 12, 50, 100, 200) in mJy per beam.

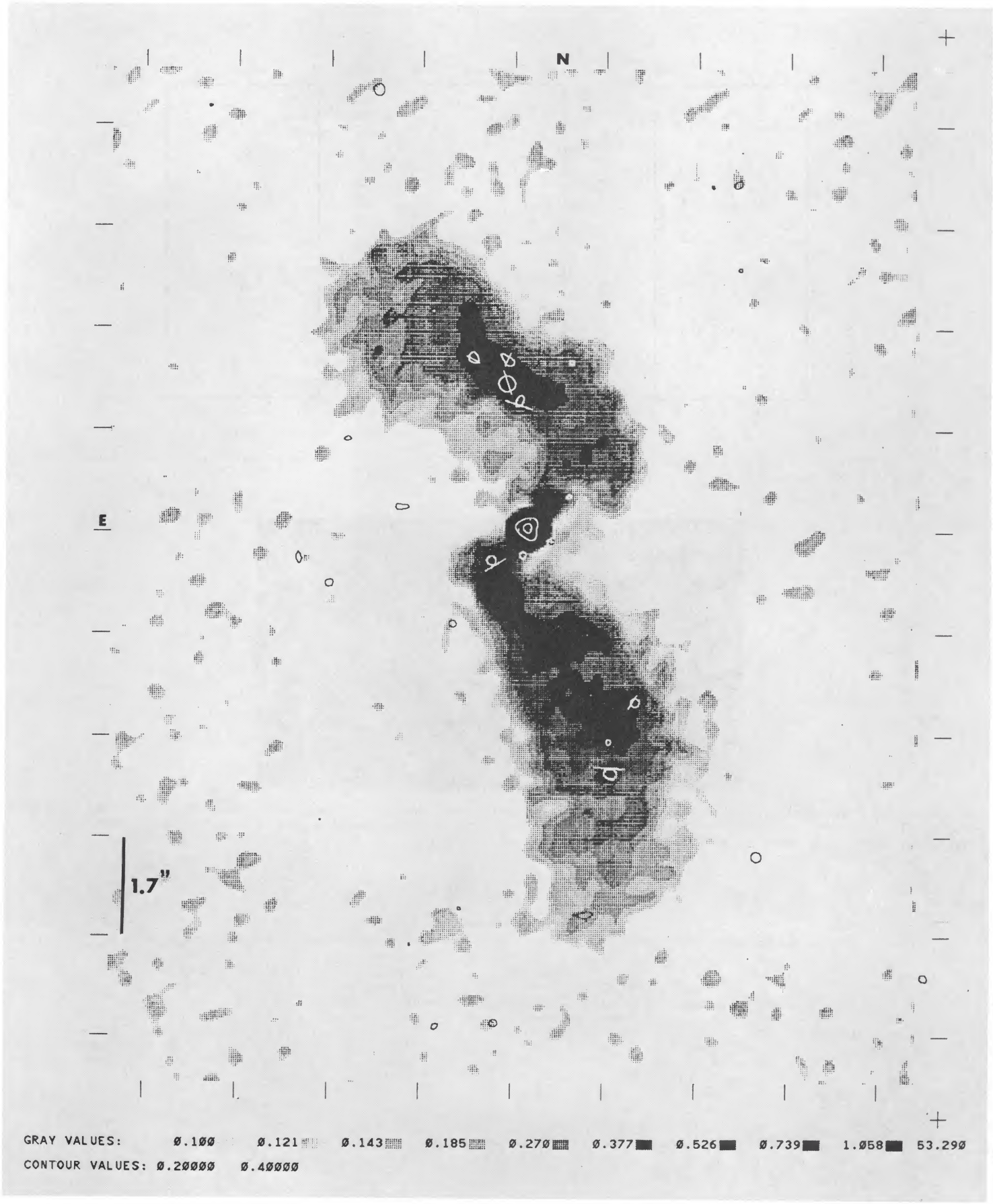

FIG. 2*b*.—Gray scale map of 4C 26.42 observed at 6 cm with 0.″3 × 0.″3 resolution. The contours (0.2 and 0.4 mJy per beam) represent the polarized intensity, and the line segments represent the polarization position angles. The polarization at the nucleus is probably spurious (see text).

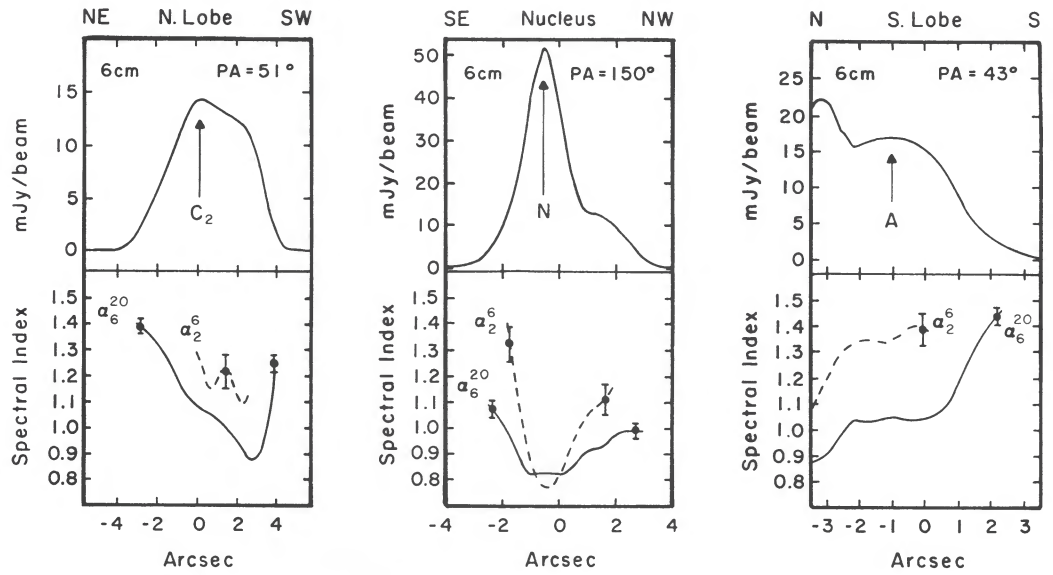

FIG. 3.—Slices through the lobes and the nucleus of 4C 26.42 of the total intensity at 6 cm (1.″3 × 1.″3 resolution) and the spectral index between 20 cm and 6 cm (α_6^{20}) and between 6 cm and 2 cm (α_2^6).

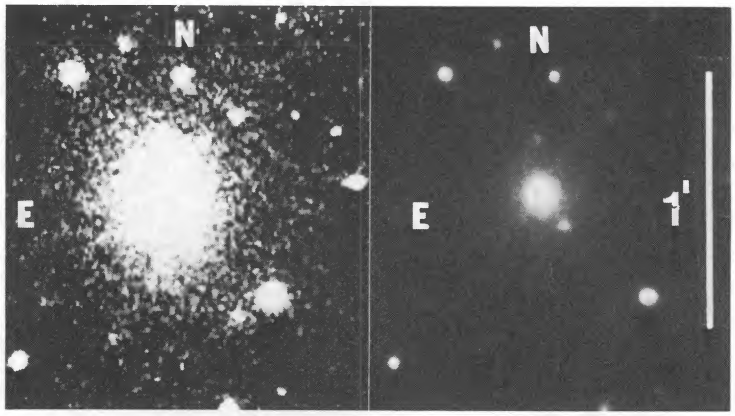

FIG. 4.—Two reproductions of the red video camera image of the cD galaxy in the cluster Abell 1795 which is identified with 4C 26.42. Each frame is 1.′5 × 1.′7. The left frame shows the large-scale structure, while the right frame shows the inner region. Most other objects in the field are galaxies and are presumably members of the cluster; one of them can be seen ~9″ southwest of the nucleus.

TABLE 4

PHYSICAL PARAMETERS (RADIO EMISSION)

Component[a]	Size[a] (arcsec)	Flux Density[a] at 6 cm (mJy)	Magnetic Field[b] (10^{-5} gauss)	Equivalent[b] Thermal Pressure $\times k^{-1}$ ($= nT$) (10^6 K cm^{-3})	Minimum[b] Energy (10^{55} ergs)	Synchrotron[c] Radiation Lifetime (10^5 yr)
B_1	0.6 × 1.0	15	13	7	2	3
N	0.05	53.5 ± 0.2	>200	>1700	<0.1	<0.06
B_2	0.2	1.7 ± 0.1	>20	>22	<0.1	<2
C_2	0.8 × 1.1	21	12	6	3	4
S. lobe	2 × 5.5	81 ± 6	6	1.5	20	8
N. lobe	2 × 5.5	70 ± 5	6	1.5	20	8
Total	2 × 12	225 ± 16	6	1.5	50	7

[a] See Fig. 2 and § III*a*(iii).
[b] See § III*a*(iii).
[c] At 6 cm.

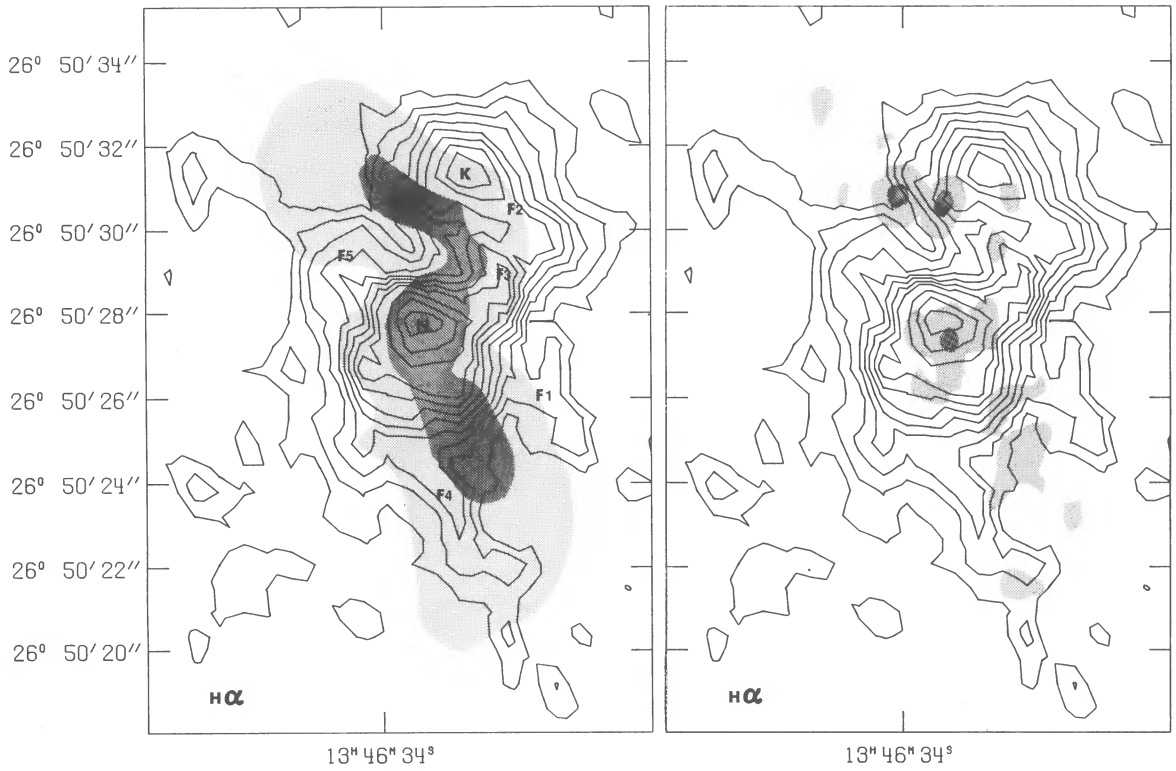

FIG. 5.—Contour representation of the Hα + [N II] line emission (1″ seeing) associated with 4C 26.42. Contour values, increasing linearly, are arbitrarily scaled. Various components are labeled, and their corresponding Hα + [N II] fluxes are listed in Table 5. The shaded areas represent the total intensity (*left*) and the polarized intensity (*right*) at 6 cm with 1.″3 × 1.″3 resolution.

3. In general, the source is depolarized at 6 cm in regions where the radio and line emission overlap. (The polarization near the nucleus may be spurious; see previous section.)

Our Cryogenic Camera spectrum in position angle 162° also shows weak line emission gas extending some 45″ (~50 kpc) to the south and 10″ (~11 kpc) to the north of the nucleus (see Fig. 7). The very extended emission to the south is faint and is not seen in our video camera frame (attesting to the greater sensitivity of the Cryogenic Camera). This emission ends in a brightness enhancement (the "southern knot") which is ~5% as luminous as the nucleus in the light of Hα + [N II]. The overall extent of the emission-line system is thus at least ~60 kpc and so is comparable in size to the NGC 1275 filament system (Lynds 1970). This extended emission to the south has been imaged by Cowie *et al.* (1983), who find it to be a narrow, filamentary structure

TABLE 5

PHYSICAL PARAMETERS (OPTICAL EMISSION)

Component[a]	Summation Area[a] (arcsec)	Hα + [N II] Flux[a] (10^{-15} ergs cm^{-2} s^{-1})	Total Emission-Line Luminosity[b] (10^{42} ergs cm s^{-1})	Filling Factor[b,c] $(n_{EL}/100)^{-2}$	Ionized Hydrogen[b,c] $10^7(n_{EL}/100)^{-1}\ M_\odot$
S. lobe:					
F_1	1.7 × 1.7	1.3	1.0 total S. lobe	2×10^{-4}	2.2
F_2	1.7 × 5.8	5.1	...	...	...
Nucleus	1.7 × 1.7	9.2	1.4	3×10^{-2}	3.1
N. lobe:					
F_2	2.3 × 4.6	15.9	5.2 total N. lobe	7×10^{-4}	11.4
F_3	2.3 × 2.3	9.4	...	...	...
F_5	2.3 × 2.3	4.1	...	...	...
K.....	1.7 × 1.7	5.2	...	...	...
Total ...	entire source	71	11	...	24

[a] See Fig. 6. Note that [N II] contributes only 30% to these fluxes in our bandpass.

[b] Assuming case B recombination; we estimate that the total luminosity of all emission lines is approximately 20 × Hα + [N II].

[c] Normalized to a density in the line-emitting gas (n_{EL}) of 100 cm^{-3}.

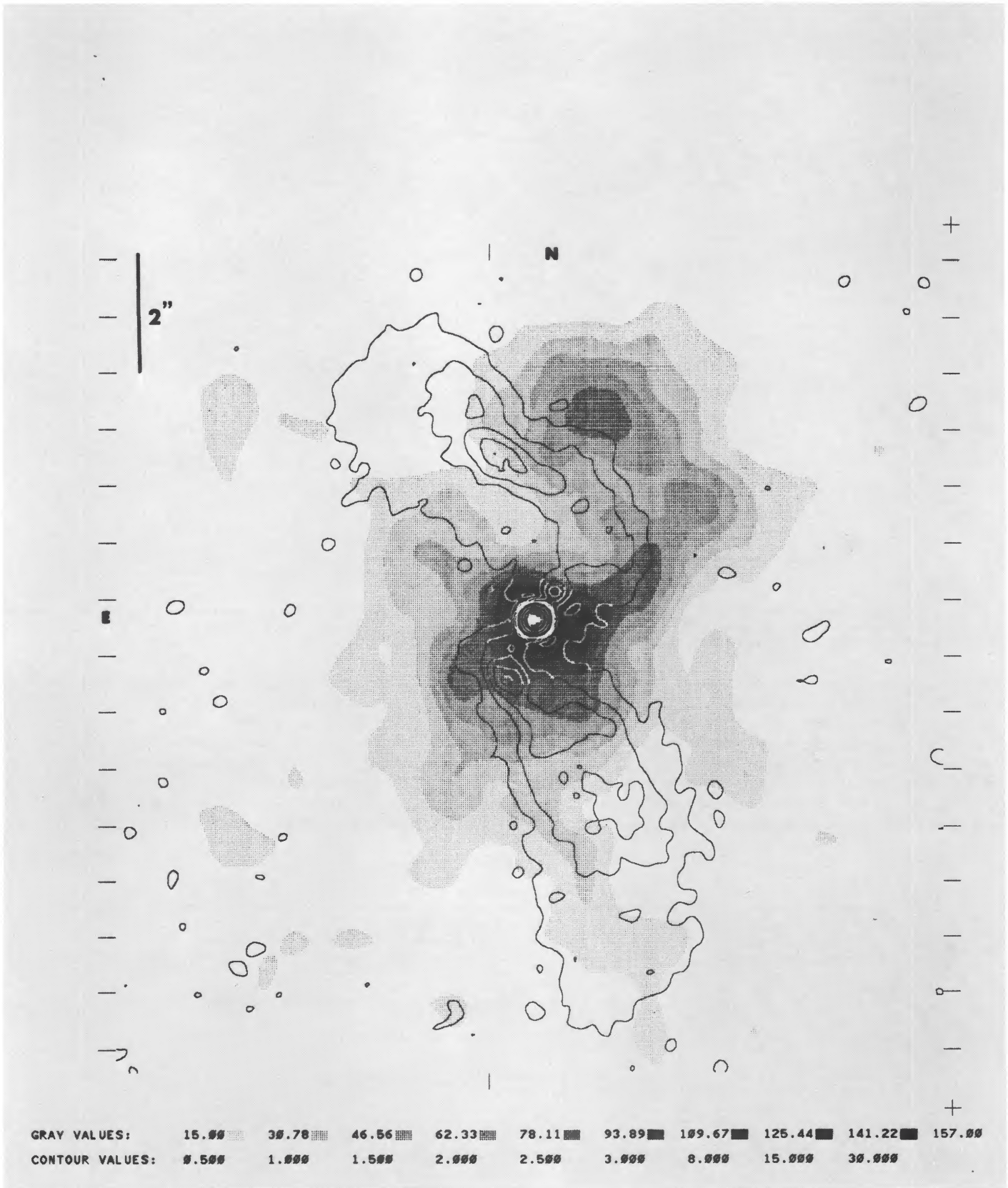

FIG. 6.—Gray scale representation of the Hα + [N II] line emission (1″ seeing) with contours of the 6 cm (0.″3 × 0.″3) total intensity superposed. Contour values are 0.5, 1, 1.5, 2, 2.5, 3, 8, 15, and 30 mJy per beam.

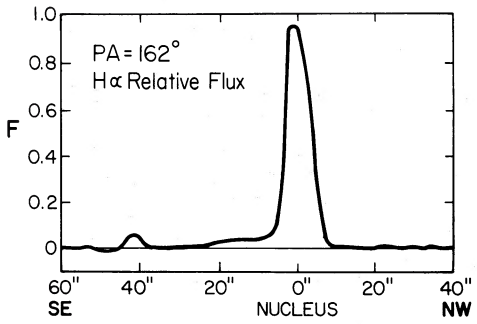

FIG. 7.—The relative intensity of the Hα + [N II] emission lines along a slit position angle 162° from our Cryogenic Camera data. Note the very extended line emission to the south. The scale along the vertical axis is arbitrary.

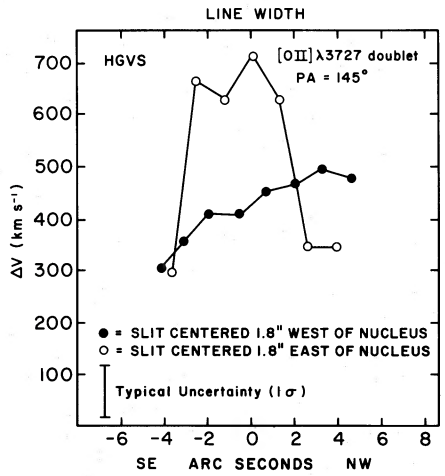

FIG. 9.—The velocity widths of the [O II] doublet lines after deblending (see text).

somewhat misaligned with a radial orientation. No large-scale radio counterpart to this faint, extended line emission to the south is evident in our radio maps.

ii) *Kinematics*

We have inferred kinematical information about the emission-line gas in 4C 26.42 from the long-slit spectra. The center velocities and line widths are shown in Figures 8 and 9. We conclude that:

1. The bulk velocities of the gas are $\lesssim 500$ km s^{-1}.
2. There is no rotation: both northward and southward, the lines are blueshifted by 400–500 km s^{-1} with respect to the nucleus. The southern knot (~ 50 kpc to the southeast) is blueshifted by ~ 200 km s^{-1} relative to the nuclear gas.
3. The velocity widths are ~ 500 km s^{-1} in the nucleus, reach 600–700 km s^{-1} southeast of the nucleus, and are 300 km s^{-1} elsewhere.

iii) *Spectrum*

Our HGVS and Cryogenic Camera long-slit data, while only roughly flux calibrated, clearly show the emission-line spectrum in 4C 26.42 to resemble that of the gas in the cluster-dominant active galaxies M87 (Ford and Butcher 1979), NGC 1275 (Kent and Sargent 1979), NGC 6166 (unpublished data), and 3C 317 (Cohen and Osterbrock 1981). In particular, the spectrum is dominated by lines from neutral or singly ionized species (e.g., H I, O I, S II, O II, N II), while lines from highly ionized species (e.g., Ne V, Ne III, He II, O III) are weak or absent (Table 6). The Hα/Hβ ratios indicate that reddening by dust is not large. The spectra of the bright emission-line gas near the nucleus and of the faint southern knot are rather similar to one another.

Cowie *et al.* (1983) did not detect the [S II] λλ6717, 6731 lines in 4C 26.42 and set an upper limit to the λ6717 strength of $\leq 20\%$ Hα. In contrast, we find that [S II] λ6717 is $\sim 50\% \pm 10\%$ of Hα within $\sim 4''$ of the nucleus in P.A. = 160° and is $\sim 20\% \pm 10\%$ of Hα in the distant southern knot. Our data near the nucleus have high signal-to-noise ratios, so we are not able to account for the result of Cowie *et al.* They note that their [S II] image is of significantly lower quality than their Hα image. Perhaps they have underestimated their limit on the [S II]/Hα ratio.

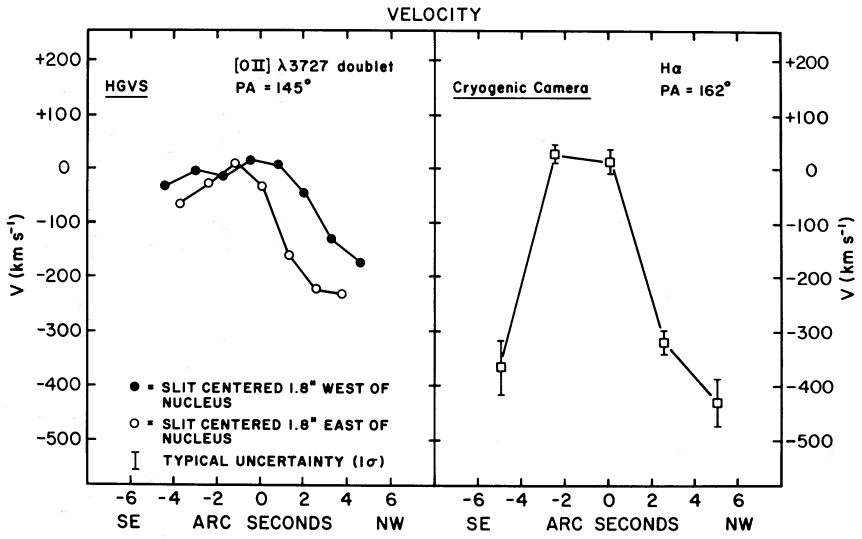

FIG. 8.—The velocity of the [O II] λ3727 doublet (*left*) and Hα (*right*) emission lines using, respectively, the HGVS and the Cryogenic Camera at slit positions as indicated. The zero point along the vertical scale (velocity) is within 100 km s^{-1} of the systemic velocity of the galaxy (18,887 km s^{-1}).

TABLE 6

RELATIVE LINE STRENGTHS

Emission Line	Central Region	Distant Southern Knot
[S II] λλ6717, 6731	27 ± 2	10 ± 3
[N II] λ6584	25 ± 2	15 ± 3
Hα	33 ± 2	25 ± 3
[O I] λ6300	10 ± 2	6 ± 3
[O III] λ5007	6 ± 2	<5
Hβ	10	10

NOTE.—In addition to the quoted errors, the relative intensities of the bluemost vs. the redmost lines are uncertain by 20%–30% (see text).

iv) *Physical Parameters*

Assuming a case B recombination spectrum (Osterbrock 1974), we have derived the total luminosity, filling factor, and mass of the ionized hydrogen (Table 5).

From the [S II] λ6717/λ6731 intensity ratio, $n_e \leq 300$ cm^{-3}. However, n_e may also be estimated by assuming pressure balance between the emission-line gas and the radio source. In 3C 305 detailed spectroscopic and radio observations have provided independent evidence that the radio source and emission-line gas are in pressure equilibrium (Heckman *et al.* 1982), and recent observations of 3C 277.3 (van Breugel *et al.* 1984*b*) suggest that this may also hold for the bright knot near the nucleus of this source.

Assuming pressure balance also occurs in the lobes of 4C 26.42, then on average $nT \approx 1.5 \times 10^6$ K cm^{-3} (Table 4). Within a factor of ~ 2, $T \approx 2 \times 10^4$ K for the line-emitting gas so that $n_e \approx 40$–150 cm^{-3}. For comparison, $n_e \approx 10^3$ cm^{-3} in M87 (Ford and Butcher 1979) and the near-nuclear low-velocity filaments in NGC 1275 (Kent and Sargent 1979). We have normalized all the parameters in Table 5 which involve n_e to a density of 100 cm^{-3}, remembering that this value may be in error by at least a factor of 3.

IV. DISCUSSION

a) Environment

4C 26.42 is identified with the very luminous ($M_v = -23$) cD galaxy at the center of the rich cluster of galaxies Abell 1795 (e.g., Owen, Rudnick, and Peterson 1977). This cluster has a richness class of 1 and a Bautz-Morgan type of I (Leir and van den Bergh 1977) and is one of the more powerful cluster X-ray sources known, with an X-ray luminosity of $\sim 8.5 \times 10^{44}$ ergs s^{-1} in the 0.5–4.5 keV band (Jones *et al.* 1979). The X-ray gas in Abell 1795 has been shown to be centrally condensed at the location of the dominant galaxy associated with 4C 26.42 (Jones *et al.* 1979; Forman-Jones 1982).

This morphology and the spectrum (Mushotzky *et al.* 1981) of the X-ray emitting gas demonstrate the presence of a substantial core of cool ($T \lesssim 10^7$ K) gas, in agreement with theoretical models of a "cooling accretion flow" (e.g., Fabian and Nulsen 1977).

While detailed models are not available for Abell 1795, the conditions in the X-ray core are likely to be similar to those in the Perseus Cluster (centered on NGC 1275) and the Virgo Cluster (centered on M87). In both NGC 1275 (Mushotzky *et al.* 1981; Fabian *et al.* 1981) and M87 (Fabricant, Lecar, and Gorenstein 1980; De Young, Condon, and Butcher 1980) the thermal pressures in the core region ($r \lesssim 10$ kpc) are estimated to be approximately $nT \approx 10^6$ K cm^{-3}, the temperatures $T \approx 10^7$ K, and the densities $n \approx 0.1$ cm^{-3}. Such a pressure would be adequate to statically confine the diffuse lobes of 4C 26.42 (cf. Table 4). Thermal confinement would be consistent with (1) the absence of strong radio hot spots (which are generally interpreted as ram-pressure confined regions), (2) the steep radio spectrum (interpreted as being due to an aging population of relativistic electrons), and (3) our assumption of pressure equilibrium between the radio source and the clumpy emission-line gas (§ III*b*[iv]) through mutual pressure balance with a hot intercloud medium (the X-ray core).

b) Emission-Line Gas

i) *Origin*

The cooling halo gas provides a reservoir from which still cooler ($T \approx 10^4$–10^5 K) optical emission-line gas can be formed. A temperature of $\sim 10^7$ in the X-ray core would be consistent with a temperature one would derive by interpreting the kinematics of the optical emission-line gas in terms of material which has condensed out of a hotter medium ($V_{\rm clouds} \approx V_{\rm sound}$). The cooling time for the gas ($T \approx 10^7$ K, $nT \approx 10^6$ K cm^{-3}) would be $\sim 2 \times 10^7$ yr, comparable to both the radio source lifetime of $\sim 2 \times 10^7$ yr (assuming it to be the ratio of the total minimum energy and the current total radio luminosity) and the "crossing time" of the emission-line region of $\sim 4 \times 10^7$ yr (the ratio of the size of the region and a typical velocity of ~ 300 km s^{-1}). Thus, a steady state situation in which cooling, inflowing X-ray gas both fuels the activity in the nucleus (Burns, Gregory, and Holman 1981) and provides fresh emission-line gas is possible.

The spectrum of the emission-line gas—interpreted within the context of shock heating (e.g., Dopita 1978) or photoionization (e.g., Ferland and Netzer 1983)—implies roughly solar metal abundances. This expected in the accretion of a processed intracluster medium.

ii) *Ionization Source*

Although our spectroscopic data do not allow us to unambiguously determine the process which excites the gas, they do provide some information which is relevant in discriminating between various mechanisms, i.e., photoionization or shock heating.

Photoionization by a hypothetical ultraviolet tail of the extended, nonthermal radio emission—as in the Crab nebula (Kirschner 1974; Henry and MacAlpine 1982) and possibly in the jet of 3C 277.3 (Miley *et al.* 1981)—is unlikely since the estimated total emission-line luminosity ($\sim 10^{43}$ ergs s^{-1}) is much greater than the extrapolated Lyman continuum luminosity ($\sim 10^{41}$ ergs s^{-1}) in such a case. The radio-to-ultraviolet spectrum would have to be significantly flatter than the radio spectrum, quite unlike the situation in radio jets (Butcher, van Breugel, and Miley 1980) or the Crab nebula (Kirshner 1974).

On the other hand, by comparing the energy spectrum (between 3100 and 12000 Å) of 4C 26.42 with that of a standard, nonactive elliptical galaxy, Wilkinson, Hine, and Sargent (1981) found that there may be enough *nuclear* non-

thermal continuum to photoionize the gas. This is the situation generally thought to occur in most quasars and active galactic nuclei. While the emission-line spectrum of the gas in 4C 26.42 does not strongly resemble that of a quasar or Seyfert galaxy, it is possible to construct models of gas photoionized by a dilute "power-law" ultraviolet continuum that reproduce a low-ionization spectrum as seen in 4C 26.42 (e.g., Ferland and Netzer 1983; Halpern and Steiner 1983).

Alternatively, as we have seen in the previous section, since 4C 26.42 is embedded in a cool and dense gaseous halo, radiatively regulated accretion of this gas onto the galaxy may cause the formation of emission-line filaments similar to those observed in NGC 1275 (Burbidge and Burbidge 1965; Kent and Sargent 1979). The gas in the filaments is thought to be excited by repressurizing shocks driven by the hot surrounding gas (Cowie and Binney 1977; Fabian and Nulsen 1977). The emission-line spectrum of 4C 26.42 does in fact resemble that of shocked gas (e.g., Dopita 1978).

We can check whether the observed Hα luminosity in 4C 26.42 is consistent with such a model. Cowie, Fabian and Nulsen (1980) have expressed the expected surface brightness of Hα emission—$S(\mathrm{H}\alpha)$—of a shock-heated filament in terms of its surface area (using an equivalent filament diameter, d_f, in kiloparsecs) and the external pressure ($n_{\rm ex}\,T_{\rm ex}$):

$$S(\mathrm{H}\alpha) = 2.5 \times 10^{-6} d_f^{0.16} (10^{-6} n_{\rm ex}\,T_{\rm ex})^{1.16} \text{ ergs cm}^{-2}\text{ s}^{-1}\text{ sr}^{-1}\ .$$

From our Hα + [N II] image we estimate that the total surface area of the emission-line regions is 2.5×10^{45} cm^2. We have assumed here spherical and cylindrical symmetry where appropriate for the individual components. The equivalent diameter is then $d_f \approx 10$ kpc. Taking this and assuming a $\sim 30\%$ contribution to the Hα + [N II] luminosity from the [N II] lines (from our spectra and the known throughput of the Hα interference filter), we estimate that the average Hα surface brightness in 4C 26.42 is $S(\mathrm{H}\alpha) \sim 5 \times 10^{-6}$ ergs cm^{-2} s^{-1} sr^{-1}. For comparison, in NGC 1275, $S(\mathrm{H}\alpha) \approx 1.6 \times 10^{-5}$ ergs cm^{-2} s^{-1} sr^{-1} (Kent and Sargent 1979; Cowie, Fabian, and Nulsen 1980). This value for $S(\mathrm{H}\alpha)$ implies that the external pressure on the emission-line filaments in 4C 26.42 has to be $n_{\rm ex}\,T_{\rm ex} \sim 1.3 \times 10^6$ K cm^{-3}, which is consistent with the expected pressure in the gaseous halo near the radio source (see previous section).

Thus by analogy with NGC 1275, as well as M87, the observed line emission in 4C 26.42 may be due to radiatively regulated accretion. Determination of a high temperature ($T > 3 \times 10^4$ K) in the O III zone of emission-line gas would provide direct evidence for the importance of shock heating (e.g., Fosbury *et al.* 1978) and, thus, convincing support for the above model. Although in either of the models (photoionization by the nucleus or radiatively regulated accretion) no direct relationship between the radio continuum and optical line emission is to be expected *a priori*, the observed radio/optical correlations fit in naturally with the presence of a bright radio source like 4C 26.42 embedded in a dense, cooling X-ray core. This will be discussed further in § IV*c*.

iii) *Kinematics*

The cooling–accretion-flow model, together with the apparently large velocity difference ($+440 \pm 220$ km s^{-1}) between the cD galaxy and mean cluster velocities (Hintzen 1980; Quintana and Lawrie 1982), may explain the seemingly peculiar kinematics of the emission-line gas in 4C 26.42. The gas in the outer parts of the flow will cool within the *cluster* potential, and the velocity of this gas should thus be close to the mean cluster velocity. In the vicinity of the cD galaxy, the flow will be "captured" by the *galaxy* potential, and so the inner gas will have a velocity close to that of the cD. This agrees well with the observed emission-line kinematics. Cowie *et al.* (1983) present evidence for a similar situation in the dominant galaxy in Abell 85. We conclude that if the line-emitting gas in 4C 26.42 has a kinematic component of outflow along the radio axis, this must be small ($\lesssim 10^2$ km s^{-1}).

The broad lines in 4C 26.42 are consistent with bound motion within the galaxy potential. Equivalently, the line widths are consistent with the clouds having condensed out of a gas at $T \sim 10^6$–10^7 K (emission-line velocity dispersion $\sim$ sound speed). In 3C 305 (Heckman *et al.* 1982), and in kiloparsec-scale radio sources in general (Wilson and Willis 1980; Heckman *et al.* 1981), broad emission lines are correlated with intense radio emission. Such a connection is not clear in 4C 26.42, where all the bright regions of emission-line gas are close to regions of bright radio emission. Higher spatial resolution spectroscopy will be required to look for any detailed correlation in this regard.

Blandford and Smarr (1983) have recently suggested that cluster-dominant galaxies associated with smooth, centrally peaked X-ray sources are immersed in "black pits" (deep potential wells created by nonluminous matter). They predict in cases like 4C 26.42/Abell 1795 that the characteristic velocity of material in the "pit" should rise rapidly from several hundred km s^{-1} in the galaxy nucleus to a value close to the cluster velocity dispersion (~ 1600 km s^{-1} in A1795, according to Quintana and Lawrie 1982) by radii of ~ 10 kpc. We do not see such behavior in the emission-line gas in 4C 26.42, either in terms of line width or velocity changes (cf. § III*b*[ii] and Figs. 8 and 9). The same can be said of the emission-line filaments surrounding the X-ray dominant galaxy NGC 1275 in the Perseus Cluster (e.g., Rubin *et al.* 1978).

c) Radio/Optical Comparison

i) *Morphologies*

The optical line emission along the boundaries of the radio source, the bright emission-line region close to an indentation and brightness enhancement in the radio source, and the anti-correlation between the presence of emission-line gas and radio polarization all show that the thermal gas and the radio-emitting plasma are intimately connected. Similar results have also been found in several other radio sources (see van Breugel and Heckman 1982 and Miley 1983 for summaries). This relationship is most readily interpreted by assuming that a shell of line-emitting gas surrounds the radio source and therefore appears brighter along the edges because of the longer lines of sight through the gas. The possible occurrence of emission-line filaments in the outskirts of radio sources which have a low percentage polarization was already suggested 17 yr ago (Burn 1966).

Such a shell-like geometry in 4C 26.42 has a natural explanation. Since the source is embedded in a dense X-ray core, this can result in any of the following processes:

1. With the creation of 4C 26.42 the source expanded into

the dense X-ray core, compressing and accelerating the surrounding gas, in a way perhaps similar to the interaction of a supernova remnant with the interstellar medium. Several supernova remnants are known to have optical line emission along their outer shells, and at least in some cases this is thought to be due to shock heating of (cold clouds in) the interstellar medium (e.g., Tycho, see Chevalier, Kirshner, and Raymond 1980).

2. The magnetic field associated with the radio source decelerates the accreting ionized gas, resulting in relatively high gas densities near the boundaries of the source. This gas may exhibit Rayleigh-Taylor instabilities.

3. The accreting gas is sheared along the boundaries of the radio source causing Kelvin-Helmholtz instabilities.

Both the Rayleigh-Taylor and Kelvin-Helmholtz instabilities would result in entrainment of clumps of gas into the outer layers of the radio source. Meanwhile the gas cools further on a short time scale (see § IV*a*), and either photoionization by the nucleus or repressurizing shocks may result in optically observable line emission, as described in § IV*b*. The absence of bright line emission *within* the lobes would mean that either the clouds do not penetrate deeply into the source or that they quickly evaporate once inside. It is in principle possible to obtain a typical scale size of the clouds formed via instabilities from polarization observations, as we will illustrate in § IV*c*(ii).

The bright emission-line region near the small indentation in the northern lobe of 4C 26.42 (C_2; Figs. 2*a*, 6) is most easily explained by analogy to the model proposed by De Young, Condon, and Butcher (1980) for the emission-line filaments in M87: northward motion of 4C 26.42 coupled to an accretion flow distorts the radio structure upstream until the ram pressure on the source due to the motion is balanced by the internal pressure of the radio plasma. For plausible parameters in the X-ray core ($n \approx 0.1$ cm^{-3}) and the galaxy velocity (~ 400 km s^{-1}), the ram pressure is $\sim 2 \times 10^6$ K cm^{-3}, i.e., comparable to the static external thermal pressure. The total pressure on the northern part of the source ($\sim 4 \times 10^6$ K cm^{-3}) is balanced by the higher internal pressure at the compressed region (C_2; Table 4). The converging accretion flow and larger pressure at this location result in higher gas densities and shorter cooling times than elsewhere, causing the observed enhanced optical line emission.

Finally, we believe that the **Z**-shaped structure of 4C 26.42, which is characteristic of so many radio sources, may be due to a wobbling jet axis (e.g., Gower *et al.* 1982). The precession of the nuclear spin (jet ejection) axis is predicted on several grounds in galaxies which have experienced a recent merger (e.g., Begelman, Blandford, and Rees 1980; Rees 1978). Of course, cD galaxies like the parent of 4C 26.42 are prime suspects for such "galactic cannibalism" (e.g., McGlynn and Ostriker 1980). Alternative models for the **Z**-shape are less attractive. As summarized by van Breugel and Heckman (1982), emission-line gas is often associated with sharp bends in the radio source, suggesting a deflection of the radio jet through a collision with dense material. In 4C 26.42 such a scenario would require a fortuitous distribution of ambient material to produce a nice **Z**-symmetry. For the beam refraction model of Henriksen, Vallée, and Bridle (1981) to be applicable, large projection effects must be invoked because the outer lobes of 4C 26.42 are aligned with the major axis of the galaxy, opposite to what would be expected in such a model. We also note that 4C 26.42 has no nearby companion galaxies of comparable brightness. Thus, it is unlikely that the galaxy has recently been "tidally torqued" through $\sim 90°$ as the radio morphology would require for the Wirth, Smarr, and Gallagher (1982) model to be applicable.

ii) *Polarization*

We have argued in the previous sections that 4C 26.42 is surrounded by a dense and clumpy gaseous shell. Polarized radio emission propagating through this irregular "Faraday screen" will be rapidly depolarized, but the observed polarization should rise when the map resolution is smaller than the typical clump size (Burn 1966). These properties are consistent with our available polarization information (§ III*a*[ii]). Assuming that the Faraday depth (Φ) fluctuates at random throughout the magnetoionic medium in the shell, with a scale size smaller than the observing beam, then (Burn 1966; Gardner and Whiteoak 1966)

$$P(\lambda) = P(0) \exp(-A\lambda^4),$$

where $P(\lambda)$ is the percentage polarization at wavelength λ, $P(0)$ is the percentage polarization at zero wavelength ("intrinsic" polarization along the line of sight through the radio source), and A is a parameter which depends on the typical Faraday depth of the fluctuations (Φ_f), their scale size (d_f), and the thickness of the shell (d_s).

We can briefly evaluate the consequences of dispersing fluctuations which fill the entire shell. Then (Burn 1966),

$$A = 2\Phi_f^2 d_f^{-1} d_s,$$

where $\Phi_f = 8.1 \times 10^5 (n_e B_{11})_f d_f$ rad m^{-2} (d_f and d_s in parsecs). Here, B_{11} is the magnetic field along the line of sight through the cell (in gauss), and the wavelength λ is in meters.

We can consider the following two extreme situations: the Faraday screen consists predominantly either of irregularities in the hot (10^7 K), X-ray emitting gas or of clouds and filaments of the cool (10^4–10^5 K), optical line emitting gas.

For the purpose of illustration assume, in the first case, $n_e \approx 0.1$ cm^{-3}, $B \approx 10^{-4}$ G (Table 4), $d_s \lesssim 500$ pc (Fig. 6), $P(\lambda = 6\,\text{cm}) \approx 3\%$, and $P(0) \approx P(\lambda = 2\,\text{cm}) \approx 45\%$ (§ III*a*[ii]). We then find a typical scale size for the irregularities in the hot gas of 10 pc $\leq d_f \leq$ 200 pc (at the few locations where polarization could be measured). In the second case, the gas density is $n_e \approx 10^2$ cm^{-3} (§ III*b*[iv]), which implies a scale size for the line-emitting clouds of 10^{-5} pc $\leq d_f \leq$ 200 pc. In both cases the upper limits are set by half the beam size at 6 cm (0.″15; Fig. 2*b*). The strong increase in the local percentage polarization at 6 cm when the resolution was improved from ~ 1.6 to ~ 0.4 kpc might indeed indicate that some of the "Faraday cells" are a few hundred pc in size in 4C 26.42. For comparison, the largest optical and radio filaments in the Crab nebula have sizes of 0.01–0.5 pc (Trimble 1968; Swinbank 1980).

Presumably the situation in 4C 26.42 will be more complex (e.g., the line-emitting gas may only partially cover the radio source). Then a more complicated Faraday dispersion relationship must be used which contains the cloud covering factor (see Burn 1966). This factor might be estimated once high-resolution optical observations become available (using the Space Telescope).

Although the above numerical examples are intended to be

illustrative only, they show that polarization observations of radio sources with associated optical line emission like 4C 26.42 may yield direct information on scale sizes of instabilities, or turbulence, in the radio source boundary layers.

V. CONCLUSIONS

We have presented radio and optical imaging and optical spectroscopic data concerning the radio galaxy 4C 26.42. These show that the (nonthermal) radio continuum and the (thermal) optical line emission in this source are intimately related. X-ray observations have shown that the cluster of galaxies Abell 1795, of which the parent cD galaxy of 4C 26.42 is the dominant member, has a cooling X-ray core centered on the cD galaxy. By analogy to models proposed for NGC 1275 and M87, it is therefore plausible that the line emission in 4C 26.42 is caused by radiatively regulated accretion. Our estimates of the Hα surface brightness, and the implied external pressure on the filaments, are consistent with such a model for 4C 26.42. Slow motion of the cD galaxy relative to the cluster is implied by our data and would explain the observed brightness asymmetries in the optical line and radio continuum emission (as in M87).

The preferential occurrence of optical line emission near the boundaries of the source is interpreted as being due to a relatively dense gaseous shell surrounding the source. Such a shell-type morphology may be caused by the accumulation of the cooling X-ray gas as it is decelerated and sheared along the radio source boundaries. This gas will be clumpy, and the shell may act as an irregular Faraday screen. Detailed polarization observations may in principle be used to put limits on the scale size of these irregularities, as is illustrated with a numerical example.

In its present state, the radio source may be in a relatively quiescent stage of its evolution, as is evidenced by its likely static pressure balance with the X-ray core, its steep radio spectrum, and its lack of bright hot spots.

The authors wish to thank the staffs at the NRAO (VLA) and KPNO for their assistance in obtaining and reducing the data. Dr. J. van de Hulst is thanked for making various computer programs available to us which were used for displaying the optical data in the initial stage of this project. We acknowledge useful discussion with D. De Young, L. Cowie, C. Jones, and E. Hu. NRAO is operated by the Associated Universities, Inc., under contract with the National Science Foundation. KNPO is operated by the Association of Universities for Research in Astronomy, Inc., also under contract with the National Science Foundation. T. H. acknowledges the financial support of the General Research Board for the University of Maryland and NSF grant AST 82-16553, and G. K. M. acknowledges partial travel support from NATO grant 828.

REFERENCES

Balick, B., and Heckman, T. M. 1983, *Ap. J.* (*Letters*), **265**, L1.
Begelman, M. C., Blandford, R. D., and Rees, M. J. 1980, *Nature*, **287**, 307.
Blandford, R. D., and Smarr, L. 1983, preprint.
Bridle, A. H., and Fomalont, E. B. 1978, *A.J.*, **83**, 704.
Burbidge, E. M., and Burbidge, G. R. 1965, *Ap. J.*, **142**, 1351.
Burn, B. J. 1966, *M.N.R.A.S.*, **133**, 67.
Burns, J. O., Gregory, S. A., and Holman, G. D. 1981, *Ap. J.*, **250**, 450.
Butcher, H. R., van Breugel, W., and Miley, G. K. 1980, *Ap. J.*, **235**, 749.
Chevalier, R. A., Kirshner, R. P., and Raymond, J. C. 1980, *Ap. J.*, **235**, 186.
Cohen, R. D., and Osterbrock, D. E. 1981, *Ap. J.*, **243**, 81.
Colla, G., Fanti, C., Fanti, R., Gioia, I., Lari, C., Lequeux, J., Lucas, R., and Ulrich, M.-H. 1975, *Astr. Ap.*, **38**, 209.
Cowie, L. L., and Binney, J. 1977, *Ap. J.*, **215**, 723.
Cowie, L. L., Fabian, A. C., and Nulsen, P. E. J. 1980, *M.N.R.A.S.*, **191**, 399.
Cowie, L. L., Hu, E. M., Jenkins, E. B., and York, D. G. 1983, *Ap. J.*, **272**, 29.
De Young, D. S., Condon, J. J., and Butcher, H. R. 1980, *Ap. J.*, **242**, 511.
Dopita, M. 1978, *Ap. J. Suppl.*, **37**, 117.
Fabian, A. C., Hu, E. M., Cowie, L. L., and Grindlay, J. 1981, *Ap. J.*, **248**, 47.
Fabian, A. C., and Nulsen, P. E. J. 1977, *M.N.R.A.S.*, **180**, 479.
Fabricant, D., Lecar, M., and Gorenstein, P. 1980, *Ap. J.*, **241**, 552.
Ferland, G. J., and Netzer, H. 1983, *Ap. J.*, **264**, 105.
Ford, H. C., and Butcher, H. R. 1979, *Ap. J. Suppl.*, **41**, 147.
Forman-Jones, C. 1982, private communication.
Fosbury, R. A. E., Mebold, U., Goss, W. M., and Dopita, M. A. 1978, *M.N.R.A.S.*, **183**, 549.
Gardner, F. F., and Whiteoak, J. B. 1966, *Ann. Rev. Astr. Ap.*, **4**, 245.
Gower, A. C., Gregory, P. C., Hutchings, J. B., and Unruh, W. G. 1982, *Ap. J.*, **262**, 478.
Halpern, J., and Steiner, J. 1983, *Ap. J.* (*Letters*), **269**, L37.
Heckman, T. M. 1981, *Ap. J.* (*Letters*), **250**, L59.
Heckman, T. M., Miley, G. K., Balick, B., van Breugel, W. J. M., and Butcher, H. R. 1982, *Ap. J.*, **262**, 529.
Heckman, T. M., Miley, G. K., Butcher, H. R., and van Breugel, W. J. M. 1981, *Ap. J.*, **247**, 403.
Henriksen, R. N., Vallée, J. P., and Bridle, A. H. 1981, *Ap. J.*, **249**, 40.
Henry, J. P., and MacAlpine, G. M. 1982, preprint.
Hintzen, P. 1980, *A.J.*, **85**, 626.
Jones, C., Mandel, E., Schwarz, J., Forman, W., Murray, S. S., and Harnden, F. R. 1979, *Ap. J.* (*Letters*), **243**, L21.
Kent, S. M., and Sargent, W. L. M. 1979, *Ap. J.*, **230**, 667.
Kirshner, R. P. 1974, *Ap. J.*, **194**, 323.
Leir, A. A., and van den Bergh, S. 1977, *Ap. J. Suppl.*, **34**, 381.
Lynds, C. R. 1970, *Ap. J.* (*Letters*), **159**, L151.
McGlynn, T. A., and Ostriker, J. P. 1980, *Ap. J.*, **241**, 915.
McKee, J. D., Mushotzky, R. F., Boldt, E. A., Holt, S. S., Marshall, F. E., Pravdo, S. H., and Serlemitsos, P. J. 1980, *Ap. J.*, **242**, 843.
Merkelijn, J. K. 1972, *Australian J. Phys.*, **25**, 451.
Miley, G. K. 1983, preprint.
Miley, G. K., Heckman, T. M., van Breugel, W. J. M., and Butcher, H. R. 1981, *Ap. J.* (*Letters*), **247**, L5.
Mushotzky, R. F., Holt, S. S., Smith, B. W., Boldt, E. A., and Serlemitsos, P. J. 1981, *Ap. J.* (*Letters*), **244**, L42.
Muxlow, T. W. B., and Ilyasov, Y. P. 1981, private communication.
Olsen, E. T. 1970, *A.J.*, **75**, 764.
Osterbrock, D. E. 1974, *Astrophysics and Gaseous Nebulae* (San Francisco: Freeman).
Owen, F. N., Rudnick, L., and Peterson, B. M. 1977, *A.J.*, **82**, 9.
Pacholczyk, A. G. 1970, *Radio Astrophysics* (San Francisco: Freeman).
Quintana, H., and Lawrie, D. G. 1982, *A.J.*, **87**, 1.
Rees, M. J. 1978, *Nature*, **275**, 516.
Robinson, W., Ball, W., Vokac, P., Piegorsch, W., and Reed, R. 1979, *Proc. Soc. Photo-Opt. Instrum. Eng., Instrumentation in Astronomy III*, **172**, 98.
Rubin, V. C., Ford, W. K., Peterson, C. J., and Lynds, C. R. 1978, *Ap. J. Suppl.*, **37**, 233.
Sargent, W. L. W. 1973, *Ap. J.* (*Letters*), **182**, L13.
Swinbank, E. 1980, *M.N.R.A.S.*, **193**, 451.
Thompson, A. R., Clark, B. G., Wade, C. M., and Napier, P. J. 1980, *Ap. J. Suppl.*, **44**, 151.
Trimble, V. L. 1968, *A.J.*, **73**, 535.
van Breugel, W. J. M., and Heckman, T. M. 1982, in *IAU Symposium 97, Extragalactic Radio Sources*, ed. D. S. Heeschen and C. M. Wade (Dordrecht: Reidel), p. 61.
van Breugel, W. J. M., Heckman, T. M., Butcher, H. R., and Miley, G. K. 1984*a*, *Ap. J.*, **277**, in press.
van Breugel, W. J. M., and Jägers, W. 1982, *Astr. Ap. Suppl.*, **49**, 529.
van Breugel, W. J. M., Miley, G. K., Heckman, T. M., Butcher, H. R., and Bridle, A. H. 1984*b*, in preparation.
Wilkinson, A., Hine, R. G., and Sargent, W. L. W. 1981, *M.N.R.A.S.*, **196**, 669.
Wilson, A. S., and Willis, A. G. 1980, *Ap. J.*, **240**, 429.
Wirth, A., Smarr, L., and Gallagher, J. S. 1982, *A.J.*, **87**, 602.

T. M. Heckman: Astronomy Program, University of Maryland, College Park, MD 20742
G. K. Miley: Sterrewacht Leiden, Postbus 9513, 2300 RA Leiden, The Netherlands
W. J. M. van Breugel: Steward Observatory, University of Arizona, Tucson, AZ 85721